Energy Generation Diversification for a Base Station Equipped with Two Solar Cells

Doris Benda, *Student Member, IEEE,* Sumei Sun, *Fellow, IEEE,* Xiaoli Chu, *Senior Member, IEEE,* Tony Q.S. Quek, *Senior Member, IEEE,* and Alastair Buckley

***Abstract*—Energy generation diversification can improve the reliability of a cellular network powered by renewable energy sources. However, not all locations provide the necessary conditions to use different types of renewable energy (e.g., wind energy and solar energy). In this paper, we investigate how energy generation diversification can be achieved if only solar energy is available for a base station (BS) equipped with two photovoltaic (PV) cells. Energy generation diversification is introduced by choosing different orientation angles at the PV cells. By jointly considering the BS geolocation, daily load profile, and energy generation diversification, we develop a Markov chain based algorithm to optimize the orientation angles of the two PV cells at the BS so that the number of user equipment (UEs) served by the BS per day is maximized. Our numerical results based on real-world BS load profiles and solar energy generation profiles show that the two PV cells of a BS with a constant load profile over a day should have opposite orientations (i.e., one eastward and the other westward); whereas for BSs deployed in business or residential areas where the BS load profile has a distinctive peak during the day, the two PV cells should be oriented toward the same direction that matches the peak of the energy generation profile with that of the BS load profile. In addition, our results show that for a BS equipped with two PV cells, the proposed PV cell orientation angle optimization algorithm can increase the number of served UEs per day by up to 12% as compared to the case that the two PV cells are oriented considering the geolocation only.**

***Index Terms*—Cellular networks, solar powered, PV cells, energy generation diversification, orientation angle, inclination angle**

I. Introduction

A. Background and Related Works

Increasing data volume and data rate requirements have led to an increasing densification of base station (BS) deployment in cellular networks [1]. As a consequence, the accumulated BS energy consumption is rising considerably. To alleviate the impact on the environment and the cost burden on cellular network operators, photovoltaic (PV) cell powered BSs have been considered for future cellular networks [2], [3].

BSs powered by renewable energy face the problem of temporal variations in the energy supply. These variations have to be managed properly to make efficient use of renewable energy. Energy generation diversification can mitigate the temporal variations in the energy supply at the BS by combining energy sources with anti-correlated energy generation profiles. Thus, the energy deficit in one profile can be compensated by an energy excess of another profile. Energy generation diversification has been studied in smart grids and conventional power grids with many papers published promoting the benefits of energy generation diversification [4]–[6]. However, these papers use different types of renewable energy (e.g., wind energy and solar energy) to achieve energy diversification. In this paper, we investigate how energy generation diversification can be achieved if only solar energy is available for a base station.

Energy generation diversification in a cellular network powered by renewable energy sources has mainly been achieved by combining wind energy and solar energy [2], [3]. The anti-correlation between solar energy and wind energy generation profiles is justified on a daily timescale by the effect that high pressure (low pressure) areas tend to be sunny (cloudy) with low (high) surface wind and on a seasonal timescale by the fact that solar (wind) energy is higher in summer (winter) for many areas [2].

Energy trading/sharing among BSs can also be interpreted as an energy generation diversification mechanism if the geographical diversity of the BS locations result in anti-correlated energy generation profiles. In [7], the authors showed that energy generation diversification via energy sharing among two BSs can achieve 80% energy saving per BS for two sinusoidal energy generation profiles with a phase shift of π.

Nonetheless, the reported existing work does not explore other options to diversify the energy generation profiles, especially when different renewable energy sources are not available or energy trading/sharing between BSs is not possible. This has motivated us to study the use of different orientation angles of PV cells to diversify the energy generation profiles at a BS.

B. PV Cell Angles

The deployment location, the time of the year, the orientation angle θ, and the inclination angle γ of a PV cell determine

Manuscript received ######; revised ######. This work was supported by the A*STAR-Sheffield Research Attachment Programme. This work was partly funded by the European Unions Horizon 2020 Research and Innovation Programme under grant agreement No 645705.

D. Benda, X. Chu and A. Buckley are with the University of Sheffield, United Kingdom, e-mail:dcbenda1@sheffield.ac.uk, x.chu@sheffield.ac.uk and alastair.buckley@sheffield.ac.uk.

D. Benda and S. Sun are with the Institute for Infocomm Research, Singapore, e-mail:studcb@i2r.a-star.edu.sg and sunsm@i2r.a-star.edu.sg.

T. Q.S. Quek is with the Singapore University of Technology and Design, Singapore, e-mail:tonyquek@sutd.edu.sg.

the daily energy generation profile and the daily energy yield of a PV cell.

The inclination angle γ is defined as the angle between a horizontal surface and the PV cell plane, and the orientation angle θ is defined with respect to the compass direction. A PV cell orientated towards the east, south, and west is defined as $\theta = -90°$, $\theta = 0°$, and $\theta = 90°$, respectively (cf. Fig. 1).

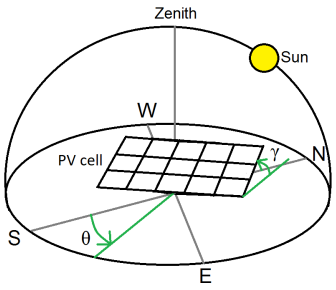

Fig. 1: Depiction of a PV cell installed with the orientation angle $\theta = -30°$ and with the inclination angle $\gamma = 20°$

The orientation angle and the inclination angle of a PV cell are usually fixed after the initial installation (cf. Fig. 2 (a)). Single-axis tracking PV cells can track the sun throughout the day via adjusting the orientation angle (cf. Fig. 2 (b)). Hence, the single-axis tracking PV cell harvests more energy per day compared to a fixed PV cell. Dual-axis tracking PV cells can track the sun throughout the day and the season (e.g., winter and summer) via adjusting both the orientation angle and the inclination angle (cf. Fig. 2 (c)). Hence, the dual-axis tracking PV cell harvests more energy per year compared to a single-axis tracking PV cell. Nonetheless sun tracking PV cells are not as commonly deployed as fixed PV cells, due to the additional parts needed (e.g. axis motor), the higher maintenance (e.g. mechanical parts like the axis and the motor break easier), and the energy needed to operate the axis motor which can be higher than the additional energy generated due to the sun tracking for some location [8]. As a result, sun tracking PV cells are not suitable for deployment at a BS. Hence, their performance metric should be interpreted as an upper bound performance for the fixed mounted PV cells in this paper.

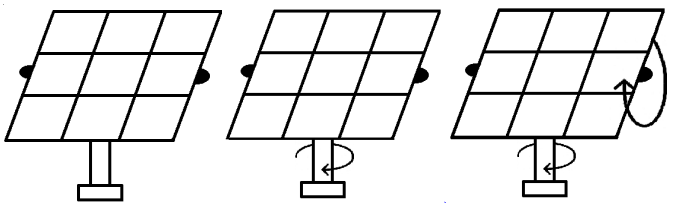

Fig. 2: Depiction of (a) a fixed PV cell, (b) a single-axis tracking PV cell, and (c) a dual-axis tracking PV cell

In case that the angle of a PV cell cannot be changed after installation, it is necessary to optimize the orientation angle of the PV cell when it is initially deployed. Without considering the need of the appliance to be powered by the PV cell, angle optimization can be done easily by choosing the default angles for the PV cell deployment area. The default inclination angle is similar to the latitude of the deployment area [9], and the default orientation angle is $0°$ and $180°$ in the northern hemisphere and in the southern hemisphere, respectively (cf. TABLE I) [9]. These default angles guarantee that the PV cell harvests the most energy on a yearly timescale among all possible orientation and inclination angles, but the energy generation profile of the PV cell may not match very well the energy consumption profile of the appliance.

TABLE I:
DEFAULT OPTIMAL ORIENTATION ANGLE θ AND INCLINATION ANGLE γ FOR DIFFERENT LOCATIONS [9]

Location	θ	γ
Northern hemisphere	$0°$	similar to the location's latitude
Southern hemisphere	$180°$	similar to the location's latitude
Equator	any orientation angle	$0°$

Optimizing the PV cell orientation (inclination) angle with consideration of the appliance energy consumption profile has been studied in [10] ([11]). The orientation (inclination) angle is optimized to achieve the best daily (yearly) match between the energy generation and consumption profiles in [10] ([11]).

Fig. 6 (a) shows the time shift of the energy generation profile of a southeast ($\theta = -45°$) and a southwest ($\theta = 45°$) facing PV cell for London in summer. Orientating a PV cell eastwards (westwards) shifts the energy generation profile towards the morning (evening) hours in the northern hemisphere. In addition, the energy generation profile of a single-axis tracking PV cell is depicted in Fig. 6 (a), which generates more energy per day than any of the fixed PV cell installations.

Deploying more than two PV cells at a BS will not increase the degree of diversity because the more the PV cell faces eastwards/westwards the more the energy generation profile is shifted towards the morning/evening hours. Therefore, two PV cells can already achieve the maximum degree of diversity by shifting one energy generation profile completely towards the morning hours and the other energy generation profile completely towards the evening hours.

C. Contributions and Organization

In this paper, we focus on a Markov chain based orientation angle optimization for a BS equipped with two PV cells. Due to the potential different orientation angles of the two fixed mounted PV cells, the energy generation profile of the BS can be diversified. The effects of considering or not considering the parameters (geolocation, energy consumption profile, energy generation diversification, and sun tracking) during the orientation angle optimization are investigated.

The main contributions of this paper can be summarized as follows:

- Development of a Markov chain based orientation angle optimization algorithm for a BS equipped with two fixed mounted PV cells with the objective to maximize the number of user equipments (UEs) served by the BS per day $\overline{S_{UE}}(\theta_1(t), \theta_2(t), \gamma)$.
- Comparison of the effectiveness of the energy generation diversification for a BS with constant load, business load, and residential load. The number of UEs served per day is used as the performance metric for the comparison.
- Comparison of the effectiveness of different PV cell orientation optimization modes (Mode 0 - 3): Optimizing the PV cell orientation angle only considering the PV cell location (Mode 0), considering the PV cell location and the energy consumption profile of the BS without energy generation diversification (Mode 1), considering the PV cell location and the energy consumption profile of the BS with energy generation diversification (Mode 2), using two single-axis tracking PV cells (Mode 3). The number of UEs served per day is used as the performance metric for the comparison.

The organization of the paper can be summarized as follows. The system model is presented in Section II. It consists of the definition of the 4 optimization modes (Mode 0 - 3) in Subsection II-A and the energy generation and consumption flows in Subsection II-B. The Markov chain based orientation angle optimization algorithms is introduced in Section III. The optimization results are discussed in Section IV whereas the effectiveness of energy generation diversification for different BS load profiles are compared in Subsection IV-B and the effectiveness of the different optimization modes are compared in Subsection IV-C. A conclusion is given in Section V.

II. System Model

Fig. 3 depicts the system model considered in this paper. It consists of an energy generation part with two identical PV cells denoted as PV cell 1 and PV cell 2, an energy storage part made of a battery, and an energy consumption part composed of a BS. The energy flow follows the arrows in Fig. 3 and can only be altered by choosing different orientation angles for one of the PV cells or both of them. All other parameters will be fixed.

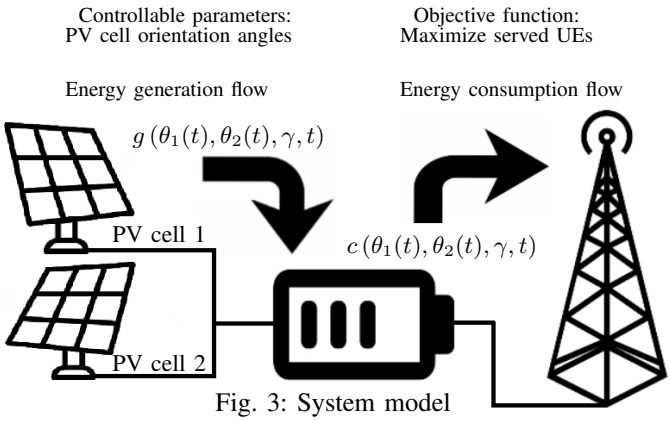

Fig. 3: System model

A. PV Cell Orientation Modes

The time is modeled in discrete time steps $t \in \{1, ..., T\}$, where T is the number of time steps per day. The PV cell orientation angles will be fixed throughout a time step but may differ between two subsequent time steps or between the two PV cells. The orientation angle of PV cell 1 and 2 at time step t is denoted as $\theta_1(t)$ and $\theta_2(t)$, respectively.

We define 4 orientation Modes, which have different restrictions on the allowed choices of the orientation angles $\theta_1(t)$ and $\theta_2(t)$. In general, a Mode with a larger index has less restrictions on the allowed choices of the orientation angles so that more orientation angles are feasible. As a result, the maximum value of the objective function may be higher at a cost of increasing the computational complexity of the optimization algorithms.

In Mode 0 (cf. Fig. 4 (a)), both PV cells are fixed mounted PV cells deployed with the default optimal orientation angle for the PV cells geolocation which is given as $0°$ and $180°$ for locations in the northern hemisphere and in the southern hemisphere, respectively. No orientation angle optimization has to be done in this mode.

In Mode 1 (cf. Fig. 4 (b)), both PV cells are fixed mounted PV cells deployed with the same orientation angle among the set $\{-90°, -60°, -30°, 0°, 30°, 60°, 90°\}$. This Mode is equivalent to deploying one PV cell with twice the surface area of PV cell 1.

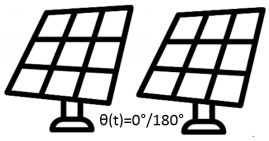

(a) Mode 0
$\theta_1(t) = \theta_2(t) = 0° \quad \forall t$
(Northern hemisphere)
$\theta_1(t) = \theta_2(t) = 180° \quad \forall t$
(Southern hemisphere)

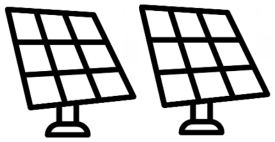

(b) Mode 1
$\theta_1(t) = \theta_2(t) =$
$\theta_1(t-1) = \theta_2(t-1) \quad \forall t$
$\theta_1(1) \in \{-90°, -60°,$
$-30°, 0°, 30°, 60°, 90°\}$

Fig. 4: PV cell orientation (a) Mode 0 and (b) Mode 1

In Mode 2 (cf. Fig. 5 (a)), both PV cells are fixed mounted PV cells deployed with an orientation angle among the set $\{-90°, -60°, -30°, 0°, 30°, 60°, 90°\}$. The orientation angle of PV cell 1 may differ from PV cell 2. Mode 2 has more degree of freedom than Mode 1. Nonetheless PV cells are more often deployed in Mode 1 because PV cells in Mode 1 can be mounted on one support structure and their physical footprint is lower, whereas PV cells in Mode 2 require two support structures.

In Mode 3 (cf. Fig. 5 (b)), both PV cells are single-axis sun tracking PV cells.

(a) Mode 2
$\theta_1(t) = \theta_1(t-1) \quad \forall t$
$\theta_2(t) = \theta_2(t-1) \quad \forall t$
$\theta_1(1) \in \{-90°, -60°, -30°, 0°, 30°, 60°, 90°\}$
$\theta_2(1) \in \{-90°, -60°, -30°, 0°, 30°, 60°, 90°$

(b) Mode 3
$\theta_1(t) = \theta_2(t) = \arg \max_{\theta \in \{-90°, -89°, \ldots, 89°, 90°\}} G(\theta, \gamma, t) \quad \forall t$

Fig. 5: PV cell orientation (a) Mode 2 and (b) Mode 3

B. Energy Generation and Consumption Flows

The two PV cells are the only energy source for the BS. The battery $b(\theta_1(t), \theta_2(t), \gamma, 0)$ is initialized with the energy level b_{begin} at the beginning of the day $(t = 0)$ by

$$b(\theta_1(t), \theta_2(t), \gamma, 0) = b_{\text{begin}}. \tag{1}$$

The harvested energy by the PV cells $h(\theta_1(t), \theta_2(t), \gamma, t)$ is calculated at each time step t by

$$h(\theta_1(t), \theta_2(t), \gamma, t) = (G(\theta_1(t), \gamma, t) + G(\theta_2(t), \gamma, t)) \cdot \eta \cdot A \cdot \tau \tag{2}$$

where $G(\theta_1(t), \gamma, t)$ and $G(\theta_2(t), \gamma, t)[\mathrm{W/m^2}]$ are the irradiance values at time step t for PV cell 1 and 2, respectively, η is the PV cell energy conversion efficiency coefficient, $A[\mathrm{m^2}]$ is the surface area of the PV cells, and $\tau[\mathrm{s}]$ is the length of one time step.

The time dependent irradiance values can be downloaded from the data base [12] on a 15-minute time resolution.

The energy generation flow $g(\theta_1(t), \theta_2(t), \gamma, t)$ at time step t is limited either by the harvested energy of the PV cells or the the remaining storage capacity of the battery by

$$\begin{aligned} g(\theta_1(t), \theta_2(t), \gamma, t) = \min\{&h(\theta_1(t), \theta_2(t), \gamma, t), \\ &b_{\max} - b(\theta_1(t-1), \theta_2(t-1), \gamma, t-1)\} \end{aligned} \tag{3}$$

where $h(\theta_1(t), \theta_2(t), \gamma, t)$ is the harvested energy by the two PV cells at time step t, $b_{\max}$ is the maximum battery capacity, and $b(\theta_1(t-1), \theta_2(t-1), \gamma, t-1)$ is residual energy in the battery from the previous time step. If the battery capacity $b_{\max}$ is exceeded, it comes to a battery overflow and the excess energy is wasted.

The available energy $a(\theta_1(t), \theta_2(t), \gamma, t)$ in time step t can be calculated by

$$\begin{aligned} a(\theta_1(t), \theta_2(t), \gamma, t) = &b(\theta_1(t-1), \theta_2(t-1), \gamma, t-1) \\ &+ g(\theta_1(t), \theta_2(t), \gamma, t) \end{aligned} \tag{4}$$

where $g(\theta_1(t), \theta_2(t), \gamma, t)$ is the energy which flows into the battery, and $b(\theta_1(t-1), \theta_2(t-1), \gamma, t-1)$ is residual energy in the battery from the previous time step.

After we know that $a(\theta_1(t), \theta_2(t), \gamma, t)$ energy is available in time step t, the consumption energy flow $c(\theta_1(t), \theta_2(t), \gamma, t)$ to the BS can be calculated. The consumption energy flow correlates with the number of UEs connected to the BS. We use either a constant load profile (cf. Fig. 6 (a)), a business load profile (cf. Fig. 6 (b)) or a residential load profile (Fig. 6 (c)) to determine the number of UEs connected to the BS. The business and residential load profile is given by [13] as typical daily load profiles for the downlink transmission.

Poisson distributions (PDs) are commonly used in cellular networks to model the UE distributions. We denote $l(t)$ as the random poisson distributed variable representing the number of UEs connected to the BS at time step t. It is generated by a Poisson process with density parameter $\lambda(t)$ as follows

$$l(t) := PD(\lambda(t)) \tag{5}$$

where $\lambda(t)$ is equivalent to the average number of UEs connected to the BS at time step t. The density parameter $\lambda(t)$ is derived from the load profiles in Figs. 6 (a) - 6 (c) as follows

$$\lambda(t) = \lambda_{\%}(\lfloor t \rfloor_h) \cdot \lambda_{\max} \tag{6}$$

where $\lambda_{\max}$ is the maximum UE density in the coverage area of the BS, $\lambda_{\%}(\lfloor t \rfloor_h)$ is the user density percentage with respect to $\lambda_{\max}$ at time step $\lfloor t \rfloor_h$ (cf. Figs. 6 (a)-6 (c)). The expression $\lfloor t \rfloor_h$ denotes that t is rounded down to the nearest full hour.

The number of served UEs $s(\theta_1(t), \theta_2(t), \gamma, t)$ at time step t is either limited by the number of connected UEs to the BS or the available energy in the battery by

$$s(\theta_1(t), \theta_2(t), \gamma, t) = \min\left\{l(t), \left\lfloor \frac{a(\theta_1(t), \theta_2(t), \gamma, t)}{c_{\text{UE}}} \right\rfloor\right\} \tag{7}$$

where $l(t)$ has been defined in (5), $a(\theta_1(t), \theta_2(t), \gamma, t)$ has been defined in (4), and c_{UE} is the average amount of energy needed to serve one UE.

The energy consumption flow $c(\theta_1(t), \theta_2(t), \gamma, t)$ at time step t is given by

$$c(\theta_1(t), \theta_2(t), \gamma, t) = s(\theta_1(t), \theta_2(t), \gamma, t) \cdot c_{\text{UE}}. \tag{8}$$

The residual energy in the battery at the end of time step t can be calculated as follows

$$\begin{aligned} b(\theta_1(t), \theta_2(t), \gamma, t) = &a(\theta_1(t), \theta_2(t), \gamma, t) \\ &- c(\theta_1(t), \theta_2(t), \gamma, t). \end{aligned} \tag{9}$$

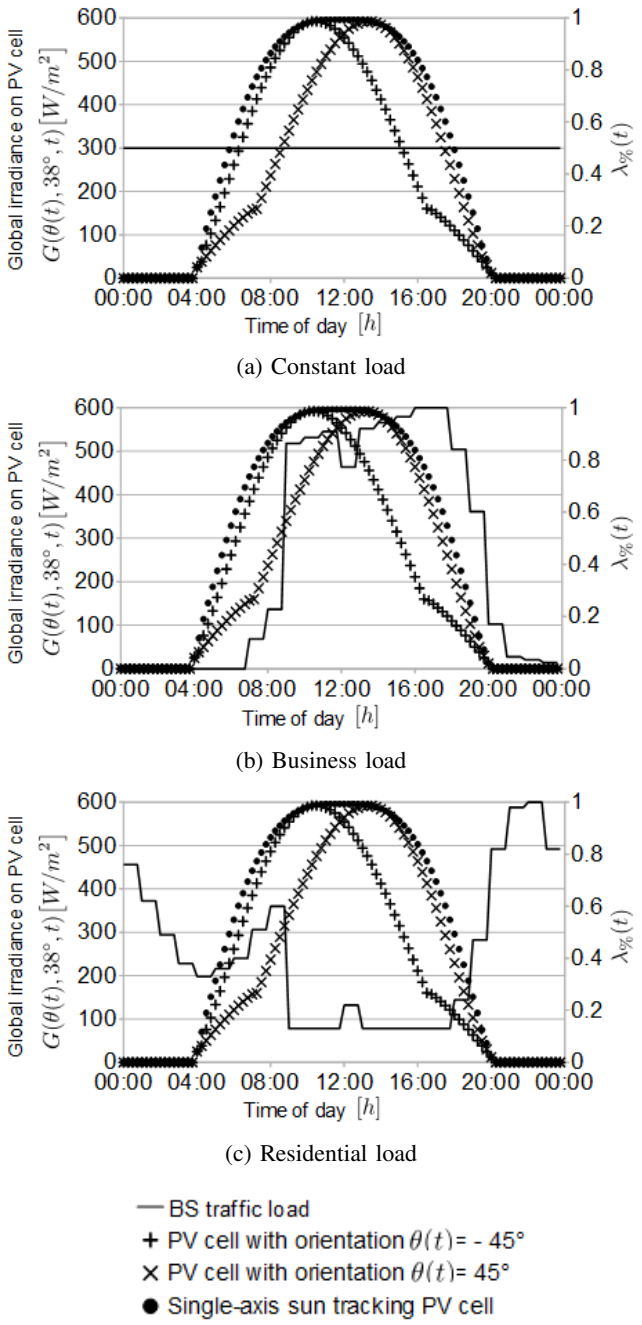

(a) Constant load

(b) Business load

(c) Residential load

Fig. 6: Constant traffic load profile, business traffic load profile, residential traffic load profile (Data source: [13]), and different energy generation profiles (Data source: [12]) for London in June

III. Markov Chain Algorithm

We use the same methods as in our previous paper [14] to transform the system model from Section II into a Markov chain based orientation angle optimization algorithm given as Algorithm 1. Algorithm 1 can run for a finite set of orientation angle pair settings $(\theta_1(t),\ \theta_2(t))$. The output $\overline{S_{\mathrm{UE}}}\,(\theta_1(t), \theta_2(t), \gamma)$ is the average total number of UEs served per day when the PV cells have $\theta_1(t)$, $\theta_2(t)$ and γ as angle settings.

The orientation angle pair setting $(\theta_1(t),\ \theta_2(t))$ with the maximum served UEs per day is considered as the optimal PV cell orientation setting $(\theta_1^*(t),\ \theta_2^*(t))$ and is given by

$$(\theta_1^*(t), \theta_2^*(t)) = \arg \max_{\substack{(\theta_1(t),\theta_2(t)) \\ \text{in Mode 0, 1, 2 or 3}}} \overline{S_{\mathrm{UE}}}\,(\theta_1(t), \theta_2(t), \gamma)\,. \tag{10}$$

Algorithm 1: Markov chain based algorithm

Input: γ, b_{begin}, $b_{\max}$, η, A, τ, T, $\lambda_{\max}$, c_{UE}, $\theta_1(t), \theta_2(t), G(\theta_1(t), \gamma, t), G(\theta_2(t), \gamma, t), \lambda_{\%}(t) \quad \forall t$
Output: $\overline{S_{\mathrm{UE}}}\,(\theta_1(t), \theta_2(t), \gamma)$

% $\mathbb{P}(l(t) = r) = \frac{\lambda(t)^r \cdot e^{-\lambda(t)}}{r!}$
% $\mathbb{P}(l(t) \geq r) = 1 - \sum_{w=0}^{r-1} \frac{\lambda(t)^w \cdot e^{-\lambda(t)}}{w!}$

% Calculation of the harvest solar energy and
% the UE density parameter for every time step
for $t = 1 : T$ **do**
  $h\,(\theta_1(t), \theta_2(t), \gamma, t) =$
    $(G(\theta_1(t), \gamma, t) + G(\theta_2(t), \gamma, t)) \cdot \eta \cdot A \cdot \tau$
  $\lambda(t) = \lambda_{\%}(\lfloor t \rfloor_h) \cdot \lambda_{\max}$
end for

% Initialization
$\mathbb{P}(b\,(\theta_1(t), \theta_2(t), \gamma, 0) = b_{\mathrm{begin}}) = 1$
$\mathbb{P}(b\,(\theta_1(t), \theta_2(t), \gamma, 0) = i) = 0$
  $\forall i \in \{0, ..., b_{\max}\} \setminus b_{\mathrm{begin}}$
$\overline{S_{\mathrm{UE}}}\,(\theta_1(t), \theta_2(t), \gamma) = 0$

for $t = 1 : T$ **do**
  % Energy generation flow
  $\mathbb{P}(b\,(\theta_1(t), \theta_2(t), \gamma, t) = i) = 0$
    $\forall i \in \{0, ..., h\,(\theta_1(t), \theta_2(t), \gamma, t) - 1\}$
  $\mathbb{P}(b\,(\theta_1(t), \theta_2(t), \gamma, t) = i) =$
    $\mathbb{P}(b\,(\theta_1(t-1), \theta_2(t-1), \gamma, t-1) = i - h\,(\theta_1(t), \theta_2(t), \gamma, t))$
    $\forall i \in \{h\,(\theta_1(t), \theta_2(t), \gamma, t)\,, ..., b_{\max} - 1\}$
  $\mathbb{P}(b\,(\theta_1(t), \theta_2(t), \gamma, t) = b_{\max}) =$
    $\sum_{r=b_{\max} - h(\theta_1(t),\theta_2(t),\gamma,t)}^{b_{\max}} \mathbb{P}(b\,(\theta_1(t-1), \theta_2(t-1), \gamma, t-1) = r)$

  % Determination of the average served UEs at time step t
  for $i = 0 : b_{\max}$ **do**
    for $r = 0 : \lfloor i / c_{\mathrm{UE}} \rfloor - 1$ **do**
      $\overline{S_{\mathrm{UE}}}\,(\theta_1(t), \theta_2(t), \gamma) = \overline{S_{\mathrm{UE}}}\,(\theta_1(t), \theta_2(t), \gamma) +$
        $r \cdot \mathbb{P}(l(t) = r) \cdot \mathbb{P}(b\,(\theta_1(t), \theta_2(t), \gamma, t) = i)$
    end for
    $\overline{S_{\mathrm{UE}}}\,(\theta_1(t), \theta_2(t), \gamma) = \overline{S_{\mathrm{UE}}}\,(\theta_1(t), \theta_2(t), \gamma) + \lfloor i / c_{\mathrm{UE}} \rfloor \cdot$
      $\mathbb{P}(l(t) \geq \lfloor i / c_{\mathrm{UE}} \rfloor) \cdot \mathbb{P}(b\,(\theta_1(t), \theta_2(t), \gamma, t) = i)$
  end for

  % Energy consumption flow
  $\mathbb{P}(b\,(\theta_1(t-1), \theta_2(t-1), \gamma, t-1) = i) = \mathbb{P}(b\,(\theta_1(t), \theta_2(t), \gamma, t) = i)$
    $\forall i \in \{0, ..., b_{\max}\}$
  $\mathbb{P}(b\,(\theta_1(t), \theta_2(t), \gamma, t) = i) = \sum_{r=0}^{\lfloor (b_{\max} - i)/c_{\mathrm{UE}} \rfloor} \mathbb{P}(l(t) = r) \cdot$
    $\mathbb{P}(b\,(\theta_1(t-1), \theta_2(t-1), \gamma, t-1) = i + r \cdot c_{\mathrm{UE}})$
    $\forall i \in \{c_{\mathrm{UE}}, ..., b_{\max}\}$
  $\mathbb{P}(b\,(\theta_1(t), \theta_2(t), \gamma, t) = i) = \sum_{r=0}^{\lfloor (b_{\max} - i)/c_{\mathrm{UE}} \rfloor} \mathbb{P}(l(t) \geq r) \cdot$
    $\mathbb{P}(b\,(\theta_1(t-1), \theta_2(t-1), \gamma, t-1) = i + r \cdot c_{\mathrm{UE}})$
    $\forall i \in \{0, ..., c_{\mathrm{UE}} - 1\}$
end for
return $\overline{S_{\mathrm{UE}}}\,(\theta_1(t), \theta_2(t), \gamma)$

IV. Results and Discussion

A. Input Parameters

TABLE II summarizes the input parameters for the Markov chain algorithm. We use London in June as a case study.

The tested angles in Mode 1 and 2 are from the set $\{-90°, -60°, -30°, 0°, 30°, 60°, 90°\}$. The default inclination angle $\gamma = 38°$ for London [12] is used in all investigated scenarios.

TABLE II:
PARAMETERS FOR THE MARKOV CHAIN ALGORITHM

Parameter	**Value**
Month (Summer)	June
Latitude (London)	$51°30'26''$ North
Longitude (London)	$0°7'39''$ West
γ	$38°$ (default inclination angle for London)
b_{begin}	$0J$
$b_{\max}$	$10000J$
η	0.15
A	0.02 m^2
τ	$15 \cdot 60s$
T	96
$\lambda_{\max}$	1.5 UEs per BS coverage area
c_{UE}	$1500J$
$G(\theta, \gamma, t)$	cf. database [12]
$G(\theta(t), \gamma, t)$	cf. database [12]
$\lambda_{\%}(t)$	cf. load profiles in Figs. 6 (a) - 6 (c)
$\theta_1(t), \theta_2(t)$ in Mode 0	$\theta_1(t) = \theta_2(t) = 0° \ \forall t$ (northern hemisphere) $\theta_1(t) = \theta_2(t) = 180° \ \forall t$ (southern hemisphere)
$\theta_1(t), \theta_2(t)$ in Mode 1	$\theta_1(t) = \theta_2(t) = \theta_1(t-1) = \theta_2(t-1) \ \forall t$ $\theta_1(1) \in \{-90°, -60°, -30°, 0°, 30°, 60°, 90°\}$
$\theta_1(t), \theta_2(t)$ in Mode 2	$\theta_1(t) = \theta_1(t-1) \ \forall t$ $\theta_2(t) = \theta_2(t-1) \ \forall t$ $\theta_1(1) \in \{-90°, -60°, -30°, 0°, 30°, 60°, 90°\}$ $\theta_2(1) \in \{-90°, -60°, -30°, 0°, 30°, 60°, 90°\}$
$\theta_1(t), \theta_2(t)$ in Mode 3	$\theta_1(t) = \theta_2(t) \ \forall t$ $\theta_1(t) = \arg \max_{\theta \in \{-90°, -89°, \ldots, 89°, 90°\}} G(\theta, \gamma, t)$

B. Comparison of the Effectiveness of Energy Generation Diversification for Different Load Profiles

TABLES III - V show the average total number of served UEs per day $\overline{S_{UE}}(\theta_1(t), \theta_2(t), 38°)$ with respect to the chosen orientation angle setting $\theta_1(1)$ and $\theta_2(1)$ in Mode 2. All the tables are symmetrical to the diagonal from the left/top to the right/bottom (cf. gray line). The values on the diagonal from the left/top to the right/bottom are the served UEs per day in Mode 1. The value in the middle of the diagonal from the left/top to the right/bottom (cf. dark gray box) is the served UEs per day in Mode 0. The optimal PV cell orientation setting $(\theta_1^*(t), \theta_2^*(t))$ is highlighted with a black box.

Figs. 7 - 9 represent the data in the tables in a graphical way. The x- and y-axes are the chosen values for $\theta_1(1)$ and $\theta_2(1)$ in Mode 2. The z-axis is the served UEs per day with respect to the chosen orientation angle setting $\theta_1(1)$ and $\theta_2(1)$ in Mode 2. Global peaks in the 3D-surface are the looked for optimal orientation angle settings for $\theta_1(1)$ and $\theta_2(1)$. All the Figs. 7 - 9 are symmetrical to the diagonal plane from the center/bottom to the center/top corner. The intersection points of the 3D-surface with the diagonal plane from the center/bottom to the center/top corner are the served UEs per day in Mode 1. The intersection point in the middle of the 3D-surface with the diagonal plane from the center/bottom to the center/top corner is the served UEs per day in Mode 0.

The x- and y-axes in Fig. 9 range from $90°$ to $-90°$ whereas they range from $-90°$ to $90°$ for a better visualization of the data in Figs. 7 and 8.

TABLE III:
SERVED UES PER DAY IN MODE 2 FOR DIFFERENT ORIENTATION ANGLE PAIRS WITH **CONSTANT LOAD**

		$\theta_1(1)$						
		$-90°$	$-60°$	$-30°$	$0°$	$30°$	$60°$	$90°$
$\theta_2(1)$	$-90°$	42.36	42.63	42.48	42.88	43.63	44.52	**44.74**
	$-60°$	42.63	42.34	42.31	42.45	43.30	44.17	44.39
	$-30°$	42.48	42.31	41.91	41.93	42.90	43.57	43.76
	$0°$	42.88	42.45	41.93	**41.65**	42.00	42.57	42.91
	$30°$	43.63	43.30	42.90	42.00	41.90	42.34	42.42
	$60°$	44.52	44.17	43.57	42.57	42.34	42.32	42.54
	$90°$	**44.74**	44.39	43.76	42.91	42.42	42.54	42.61

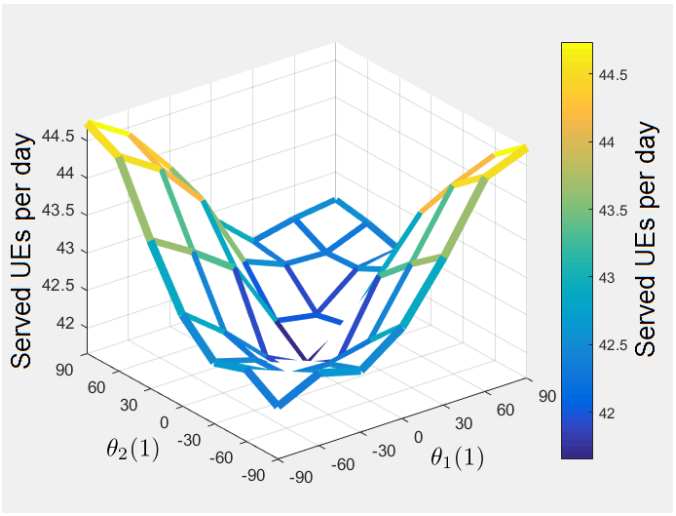

Fig. 7: Served UEs per day $\overline{S_{UE}}(\theta_1(1), \theta_2(1), 38°)$ calculated by the Markov chain algorithm in Mode 2 (Input Parameters: TABLE II with **Constant load**)

The intersection points of the 3D-surface with the diagonal plane from the center/bottom to the center/top corner in Fig. 7 show very low values, which means that using the same orientation angle for both PV cells are not favorable for constant load profiles. The global peaks at the 3D-surface at $\theta_1(1) = \pm 90°$ and $\theta_2(1) = \mp 90°$ are the optimal orientation settings which means that energy generation diversification improves the performance of the system for constant load.

TABLE IV:
SERVED UES PER DAY IN MODE 2 FOR DIFFERENT ORIENTATION ANGLE PAIRS WITH **BUSINESS LOAD**

		$\theta_1(1)$						
		$-90°$	$-60°$	$-30°$	$0°$	$30°$	$60°$	$90°$
$\theta_2(1)$	$-90°$	43.83	44.79	46.38	48.25	50.50	52.12	52.57
	$-60°$	44.79	45.8	46.93	48.78	50.90	52.56	53.05
	$-30°$	46.38	46.93	47.92	49.64	51.79	53.23	53.74
	$0°$	48.25	48.78	49.64	51.15	52.85	54.19	54.86
	$30°$	50.50	50.90	51.79	52.85	54.50	55.68	56.02
	$60°$	52.12	52.56	53.23	54.19	55.68	56.55	56.90
	$90°$	52.57	53.05	53.74	54.86	56.02	56.90	57.15

TABLE V:
SERVED UES PER DAY IN MODE 2 FOR DIFFERENT ORIENTATION ANGLE PAIRS WITH **RESIDENTIAL LOAD**

		$\theta_1(1)$						
		$-90°$	$-60°$	$-30°$	$0°$	$30°$	$60°$	$90°$
$\theta_2(1)$	$-90°$	25.71	25.69	25.27	25.11	25.22	25.44	25.60
	$-60°$	25.69	25.41	25.13	24.83	24.97	25.18	25.34
	$-30°$	25.27	25.13	24.82	24.39	24.50	24.67	24.81
	$0°$	25.11	24.83	24.39	23.79	23.62	23.71	23.84
	$30°$	25.22	24.97	24.50	23.62	23.06	23.06	23.20
	$60°$	25.44	25.18	24.67	23.71	23.06	22.90	22.96
	$90°$	25.60	25.34	24.81	23.84	23.20	22.96	23.04

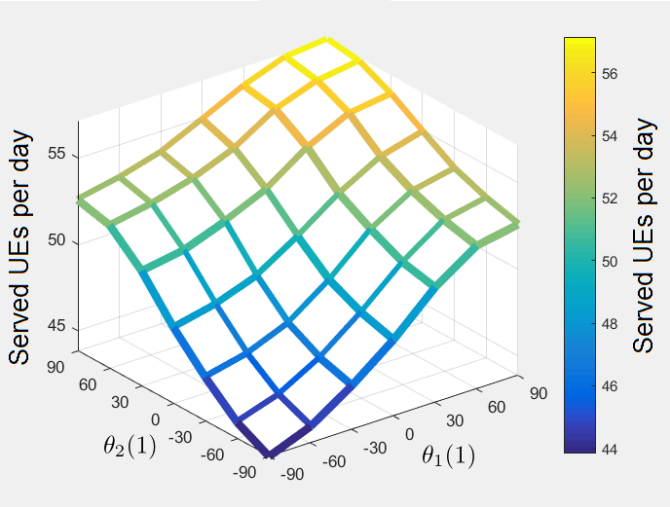

Fig. 8: Served UEs per day $\overline{S_{UE}}\,(\theta_1(1), \theta_2(1), 38°)$ calculated by the Markov chain algorithm in Mode 2 (Input Parameters: TABLE II with **Business load**)

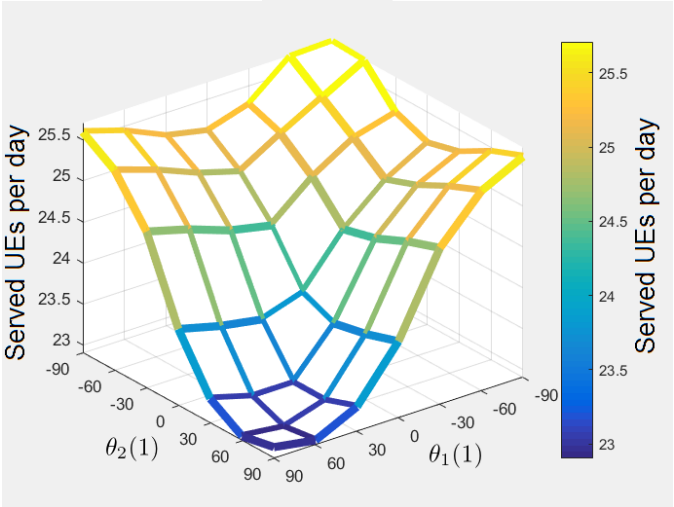

Fig. 9: Served UEs per day $\overline{S_{UE}}\,(\theta_1(1), \theta_2(1), 38°)$ calculated by the Markov chain algorithm in Mode 2 (Input Parameters: TABLE II with **Residential load**)

The peak load at the business load profile is in the evening hours. Therefore orientating both PV cells with the same orientation angle $90°$ towards the west achieves the best system performance. Energy generation diversification $\theta_1(1) = \pm 90°$ and $\theta_2(1) = \mp 90°$ improves the system performance compared to the default orientation angle setting $\theta_1(1) = \theta_2(1) = 0°$, but due to the strong peak load in the evening $\theta_1(1) = \theta_2(1) = 90°$ even further improves the system performance.

Fig. 9 is a mixture of the two effects observed in Fig. 7 and Fig. 8. On the one hand, chosing $\theta_1(1) = \pm 90°$ and $\theta_2(1) = \mp 90°$ achieves a good system performance due to the energy generation diversification. On the other hand, orientating both PV cells towards the load peak in the morning hours $\theta_1(1) = \theta_2(1) = -90°$ achieves a good system performance. The latter achieves a slightly better system performance.

Overall, the served UEs per day is the highest at the business load profile, followed by the constant load profile and at least the residential load profile. This can be explained by comparing the load profiles and the energy generation profiles in Figs. 6 (a) - 6 (c). The business load profile correlates especially in the evening hours with the energy generation profiles in Fig. 6 (b) whereas the residential load profile anti-correlates with the energy generation profiles in Fig. 6 (c).

C. Comparison of the Effectiveness of Different PV Cell Orientation Optimization Modes (Mode 0 - 3)

The comparison of the different modes are summarized in TABLE VI. Two orientation angle optimized PV cells optimized in Mode 0 (considering only the geolocation) always serve the least UEs. Two orientation angle optimized PV cells in Mode 1 (considering the geolocation and load profile) serve $2\% - 12\%$ more UEs, two orientation angle optimized PV cells in Mode 2 (considering the geolocation, load profile and energy generation diversification) serve $7\% - 12\%$ more UEs and two orientation angle optimized PV cells in Mode 3 (single-axis sun tracking PV cells) serve $12\% - 13\%$ more UEs compared to the default PV cells in Mode 0. PV cells in Mode 2 achieve the same results than Mode 1 for profiles with a distinctive peak e.g. business load and residential load and

achieve a better result for the constant profile. This shows that orientation angle optimization with energy generation diversification (Mode 2) should be conducted for load profiles similar to the constant profile whereas profiles with distinctive peak could rely on Mode 1 to reduce the computational complexity of the optimization algorithm. Mode 0 is not recommended for any load profile because it always achieves the worst performance. Mode 3 has only a slightly better performance than Mode 2 for all load profiles. Especially profiles which can achieve a good energy and consumption profile correlation after the orientation angle optimization (cf. business load profile), show a nearly equal performance in Mode 2 and 3. Therefore, Mode 2 is preferred for such profiles due to the lower CAPEX and OPEX of fixed mounted PV cells.

TABLE VI:
COMPARISON OF THE DIFFERENT MODES

		Mode 0	Mode 1	Mode 2	Mode 3
Constant load	$\theta_1^*(t)$	$0°$	$90°$	$\pm 90°$	sun tracking
	$\theta_2^*(t)$	$0°$	$90°$	$\mp 90°$	sun tracking
$\overline{S_{UE}\left(\theta_1^*(t), \theta_2^*(t), 38°\right)}$		41.65 100%	42.61 102%	44.74 107%	47.16 113%
Business load	$\theta_1^*(t)$	$0°$	$90°$	$90°$	sun tracking
	$\theta_2^*(t)$	$0°$	$90°$	$90°$	sun tracking
$\overline{S_{UE}\left(\theta_1^*(t), \theta_2^*(t), 38°\right)}$		51.15 100%	57.15 112%	57.15 112%	57.83 113%
Residential load	$\theta_1^*(t)$	$0°$	$-90°$	$-90°$	sun tracking
	$\theta_2^*(t)$	$0°$	$-90°$	$-90°$	sun tracking
$\overline{S_{UE}\left(\theta_1^*(t), \theta_2^*(t), 38°\right)}$		23.79 100%	25.71 108%	25.71 108%	26.67 112%

V. CONCLUSION

Our paper has shown that optimizing the PV cell orientation angle only considering the PV cell location (Mode 0) does not achieve a good performance in terms of the number of UEs served per day. The energy consumption profile of the BS (Mode 1 and 2) should be considered as well when optimizing the PV cell orientation angles at a BS. In addition, PV cell orientation angle optimization with energy generation diversification (Mode 2) should be considered for load profiles similar to the constant load profile whereas energy generation diversification is not necessary for peak load profiles such as business and residential load profiles. Single-axis tracking PV cells (Mode 3) have achieved a slightly better performance than the fixed mounted PV cells in Mode 2. Nonetheless, taking into account the additional CAPEX and OPEX of single-axis tracking PV cells, they are not recommended in the considered scenarios.

REFERENCES

[1] G. Piro, M. Miozzo, G. Forte, N. Baldo, L. A. Grieco, G. Boggia, and P. Dini, "Hetnets powered by renewable energy sources: Sustainable next-generation cellular networks," *IEEE Internet Computing*, vol. 17, no. 1, pp. 32–39, Jan 2013.

[2] Y. Mao, Y. Luo, J. Zhang, and K. B. Letaief, "Energy harvesting small cell networks: feasibility, deployment, and operation," *IEEE Communications Magazine*, vol. 53, no. 6, pp. 94–101, June 2015.

[3] A. Kwasinski and A. Kwasinski, "Increasing sustainability and resiliency of cellular network infrastructure by harvesting renewable energy," *IEEE Communications Magazine*, vol. 53, no. 4, pp. 110–116, April 2015.

[4] J. N. V. Lucas, G. E. Francs, and E. S. M. Gonzlez, "Energy security and renewable energy deployment in the eu: Liaisons dangereuses or virtuous circle?" *Renewable and Sustainable Energy Reviews*, vol. 62, pp. 1032 – 1046, 2016.

[5] X. Li, "Diversification and localization of energy systems for sustainable development and energy security," *Energy Policy*, vol. 33, no. 17, pp. 2237 – 2243, 2005.

[6] L. Cerovi, D. Maradin, and S. egar, "From the restructuring of the power sector to diversification of renewable energy sources: Preconditions for efficient and sustainable electricity market," *International Journal of Energy Economics and Policy*, vol. 4, no. 4, pp. 599–609, 2014.

[7] Y. K. Chia, S. Sun, and R. Zhang, "Energy cooperation in cellular networks with renewable powered base stations," *IEEE Transactions on Wireless Communications*, vol. 13, no. 12, pp. 6996–7010, Dec 2014.

[8] R. Eke and A. Senturk, "Performance comparison of a double-axis sun tracking versus fixed pv system," *Solar Energy*, vol. 86, no. 9, pp. 2665 – 2672, 2012.

[9] A. Luque and S. Hegedus, *Handbook of Photovoltaic Science and Engineering*, 2nd ed. John Wiley & Sons, 2011.

[10] D. Benda, X. Chu, S. Sun, T. Q. Quek, and A. Buckley, "Pv cell angle optimisation for energy arrival-consumption matching in a solar energy harvesting cellular network," *IEEE International Conference on Communications*, May 2017.

[11] A. H. Khan, K. R. Zafreen, A. Islam, and M. Islam, "Shifting generation of energy of solar pv using optang method-case study sandwip area," in *2015 3rd International Conference on Green Energy and Technology (ICGET)*, Sept 2015, pp. 1–5.

[12] European Commission. (2016) Photovoltaic geographical information system (pvgis). [Online]. Available: http://re.jrc.ec.europa.eu/pvgis/

[13] CelPlan. (2014) White paper - customer experience optimization in wireless networks. [Online]. Available: http://www.celplan.com/resources/whitepapers/Customer%20Experience%20Optimization%20rev3.pdf

[14] D. Benda, X. Chu, S. Sun, T. Q. Quek, and A. Buckley, "Pv cell orientation angle optimization for a solar energy harvesting base station," *IEEE Globale Communication Conference*, December 2017.